# Marangoni Convection in Weld Pool in $CO_2$-Ar–Shielded Gas Thermal Arc Welding

SHANPING LU, HIDETOSHI FUJII, and KIYOSHI NOGI

Small $CO_2$ additions of 0.092 to 10 vol pct to the Ar shielding gas dramatically change the weld shape and penetration from a shallow flat-bottomed shape, to a deep cylindrical shape, to a shallow concave-bottomed shape, and back to the shallow flat-bottomed shape again with increasing $CO_2$ additions in gas thermal arc (GTA) welding of a SUS304 plate. Oxygen from the decomposition of $CO_2$ transfers and becomes an active solute element in the weld pool and reverses the Marangoni convection mode. An inward Marangoni convection in the weld pool occurs when the oxygen content in the weld pool is over 80 ppm. Lower than 80 ppm, flow will change to the outward direction. An oxide layer forms on the weld pool in the welding process. The heavy oxide layer on the liquid-pool surface will inhibit the inward fluid flow under it and also affects the oxygen transfer to the liquid pool. A model is proposed to illustrate the interaction between the $CO_2$ gas and the molten pool in the welding process.

## I. INTRODUCTION

THE shape and penetration of gas thermal arc (GTA) welds have long been of concern, because the GTA welding process is often applied in modern industry, where high quality and precision welds are required. Surface-active elements, such as oxygen, sulfur, and selenium of group VIA, can significantly change the weld penetration in GTA welding when their concentration in the weld pool is sufficient. In order to increase weld production, the demand for automatic and precise control of the weld with deep penetration is steadily increasing. Furthermore, for welds made by automatic equipment, it is difficult to compensate for variability in the weld-pool geometry once the welding parameters have been set. Understanding and precisely controlling the effect of minor elements on the weld shape are critical for generating a satisfactory weld joint. After decades of development, there are several ways available to add surface-active elements to the weld pool. These active elements can be contained in the material to be welded,[1–6] supplied to the welding pool by a preplaced flux layer on the substrate,[7–20] or adjusted by active gaseous addition to the argon shielding gas.[21,22,23] The intentional or unintentional addition of a small amount of minor elements to the base material significantly changes the weld penetration. However, the addition of the active elements to the substrate sometimes deteriorates its mechanical properties.[22] By smearing a layer of halides or oxides on the plate surface, deep weld penetration was first obtained (active flux TIG welding or ATIG) in the 1960s at the Paton Electric Welding Institute in Ukraine (Kiev).[24] Former research results[25,26] showed that the effect of oxide fluxes on the weld-pool oxygen content and weld shape is sensitive to the flux quantity for SUS304 stainless steel containing a low oxygen content (16 ppm). The flux smearing is not easily applied in automatic welding, and is also difficult for the operator to evenly smear the effective quantity of the flux on the plate before welding, even for a heat with constant active-element content.

Compared to the ATIG welding, the investigation on the effect of gaseous additions to the argon-based shielding gas on the weld penetration and weld shape is very limited. However, the mixed gas is easily prepared and applied by automatic GTA welding in industry and is, therefore, desirable if the gas addition in a certain range can dissolve the surface-active element into the weld pool over a critical value and change the Marangoni convection mode on the pool surface and, hence, increase the weld penetration efficiently for the heat with low surface-active elements. In the 1970s, Bad'yanov[21] found that adding some gaseous fluorides ($BF_3$, $WF_6$, and $SF_6$) to the argon can increase the penetration. In the 1980s, Heiple and Burgardt[22] studied the effect of $SO_2$ shielding-gas additions on the GTA weld shape and proposed that the maximum benefit from $SO_2$ additions was achieved between 500 and 1400 ppm. However, both gaseous fluorides and sulfur dioxide are toxic, which limited their application in industry. Recently, research results showed that addition of oxygen to the argon shielding gas can significantly change the weld penetration and shape.[23]

The addition of carbon dioxide to the argon shielding gas provides a significant source of oxygen absorption for the molten weld metal. The presence of oxygen in the weld pool has been reported to have positive effects on the penetration and the shape of the weld.[12,23,25,27] The main objective of the present article is to study the effect of $CO_2$ additions to the argon-based shielding gas on the weld shape and weld penetration in GTA welding of an SUS304 stainless steel substrate. Based on the results, the mechanism for the effect of $CO_2$ additions on the weld shape is discussed.

## II. EXPERIMENTAL

Special SUS304 stainless steel plates with a sulfur content of 0.001 wt pct and oxygen content of 0.0038 wt pct were selected for the welding experiments and machined into 100 × 50 × 10 mm rectangular plates. The detailed chemical composition of the substrate is shown in Table I. Before welding, the plate was lightly ground using 80-grit flexible abrasive paper and then cleaned with acetone.

SHANPING LU, Foreign Research Fellow, HIDETOSHI FUJII, Associate Professor, and KIYOSHI NOGI, Professor, are with the Joining & Welding Research Institute, Materials Diagnosis and Life Assessment, Osaka University, Ibaraki, Osaka 567-0047, Japan. Contact e-mail: shplu@jwri.osaka-u.ac.jp or shplu@imr.ac.cn

Manuscript submitted September 18, 2003.

In order to dissolve the active element (oxygen) into the weld pool by the shielding gas, controlled levels of carbon dioxide were added to the argon-based shielding gas. All the $CO_2$-Ar gas mixtures were prepared from pure argon and premixed argon-0.92 vol pct $CO_2$ or argon-20 vol pct $CO_2$. In the experiments, the $CO_2$ content in the Ar-$CO_2$ mixed shielding gas was in the range of 0.092 vol pct (920 ppm) to 10 vol pct (100,000 ppm). Direct-current electrode-negative, automated GTA bead-on-plate welds were made in the center of the prepared plates with a mechanized system in which the testpiece was moved at a constant speed under the torch. The welding parameters are listed in Table II. The thoriated tungsten electrode was ground and the electrode gap was measured for each new bead before welding to ensure that the bead was made under the same conditions except for the shielding gas content.

After welding, all the weld beads were sectioned, and specimens for weld-shape observation were prepared using standard metallographic techniques and etched with an HCl + $Cu_2SO_4$ solution to reveal the bead shape and size. The cross sections of the weld beads were photographed using an optical microscope. The width, depth, and depth/width ratio of the weld were measured. The oxide layer on the weld surface was also observed and photographed using a laser microscope with the cross section specimens. Composition analysis of the heavy oxide layer on the bead surface was carried out by X-ray energy-dispersive spectroscopy. The oxygen content in the weld metal was analyzed using an oxygen/nitrogen analyzer. Samples for the oxygen measurement were prepared as follows: first, the oxide layer on the bead surface was removed by 400-grit abrasive paper grinding, and then the weld metal was directly cut out for use as the oxygen-analysis specimens.

**Table I. Chemical Composition of SUS304 Stainless Steel**

| Alloy Element | C | Si | Mn | Ni | Cr | P | S | O | Fe |
|---|---|---|---|---|---|---|---|---|---|
| Content (wt pct) | 0.06 | 0.44 | 0.96 | 8.19 | 18.22 | 0.027 | 0.001 | 0.0038 | bal |

**Table II. Welding Parameters**

| Parameters | Value |
|---|---|
| Electrode type | DCEN, W-2 pct $ThO_2$ |
| Diameter of electrode | 1.6 mm |
| Vertex angle of electrode | 60 deg |
| Shield gas | $CO_2$-Ar |
| Gas flow rate | 10 L/min |
| Electrode gap | 3 mm |
| Bead length | 50 mm |
| Arc voltage | 12 to 14 V |
| Welding current | 160 A |
| Welding speed | 2 mm/s |

## III. RESULTS AND DISCUSSION

### A. *Weld Shape, Oxygen Content, and Marangoni Convection*

The $CO_2$ addition to the argon-based shielding gas had a significant effect on the weld-pool shape and penetration. Cross sections of the welds are shown in Figure 1. Two cross sections at different locations in each weld are analyzed. The weld shape is quite consistent for the same weld conditions. The skewed weld shape was only observed when the $CO_2$ content in the shielding gas was 0.64 vol pct. The detailed values of the weld width and depth are given in Figure 2. For the low-$CO_2$ additions of less than 0.2 vol pct (2000 ppm), the weld is wide and shallow, as shown in Figure 1 (a1 and a2). When the $CO_2$ is in the range of 0.2 to 0.6 vol pct, the weld shape is deep and narrow, as shown in Figure 1 (b1 through b3). With a further increase in the $CO_2$, the weld pool becomes wide and shallow again. However, it is interesting to note that the shape of the weld pool is different. When the $CO_2$ addition is over 0.7 vol pct and below 4.0 vol pct, the weld bottom is concave, as shown in Figure 1 (c1 through c5). When the $CO_2$ addition is 4.0 vol pct or greater, the weld bottom is flat, as shown in Figure 1 (d1 and d2). Based on the weld cross section morphologies in Figure 1, the weld shape can be classified into four groups: (a) a shallow, flat-bottomed shape, (b) a spherical and deep cylindrical shape, (c) a shallow concave-bottomed shape, and (d) a shallow flat-bottomed shape corresponding to areas I through IV in Figure 2, respectively. Figure 2 shows that a decreasing width

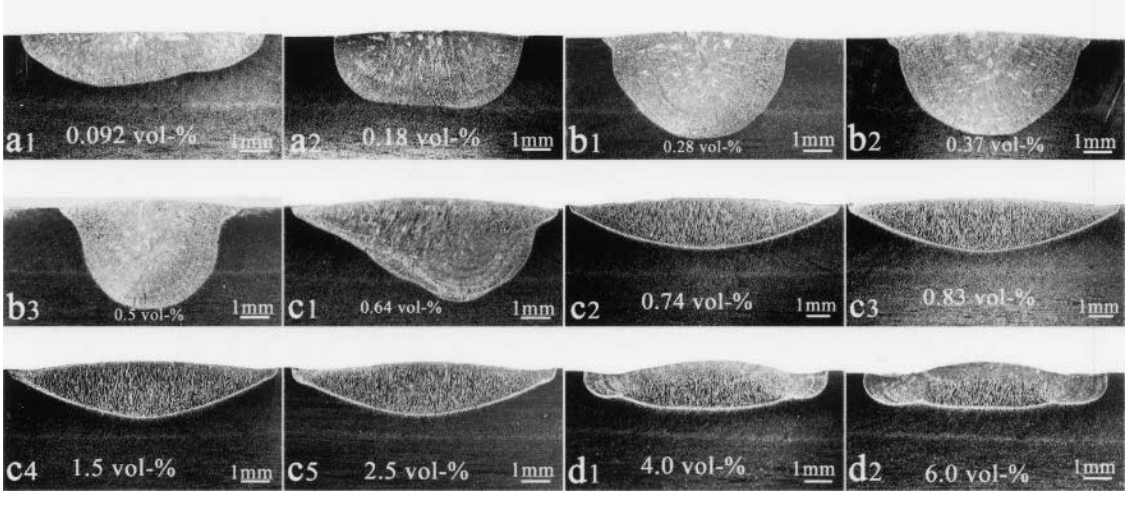


Fig. 1—Bead cross sections with different $CO_2$ additions.

corresponds to an increasing depth, and an increasing width corresponds a decreasing depth. The weld width and depth simultaneously change in opposite directions.

The oxygen analysis of the weld was carried out after welding. The weld depth/width ratio (*D*/*W*) and oxygen content in the weld are plotted *vs* the torch gas $CO_2$ content in Figure 3. A large *D*/*W* ratio, around 0.5, is obtained when the $CO_2$ concentration is in the range of 0.2 to 0.6 vol pct, as illustrated in area II in Figure 3. When out of this range, the *D*/*W* ratio decreases to 0.2. In the welding process, the $CO_2$ gas is possibly decomposed and generates oxygen under the arc. Figure 3 shows that the oxygen content in the weld initially increases with the $CO_2$ content up to 0.6 vol pct and then maintains a nearly constant value around 200 ppm for $CO_2$ contents up to 4.0 vol pct, as shown in area III in Figure 3. When the $CO_2$ content is over 4.0 vol pct, the oxygen content in the weld increases again, as shown in area IV in Figure 3

Heiple and Roper,[12] Mills *et al*.,[27] Sahoo *et al*.,[28] and Ishizaki *et al*.[29] postulated that variable weld penetration is a result of different fluid-flow modes in the welding pool, which was driven by the combination of the electromagnetic force, surface tension, buoyancy force, and impinging force of the arc plasma, and the Marangoni force is the main force

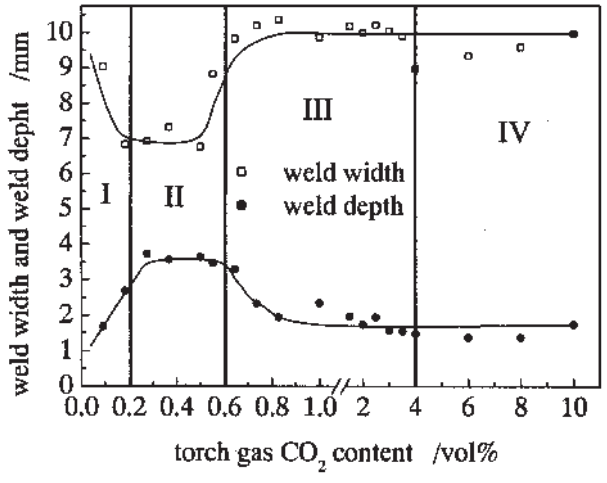


Fig. 2—Weld width and depth at different $CO_2$ additions.

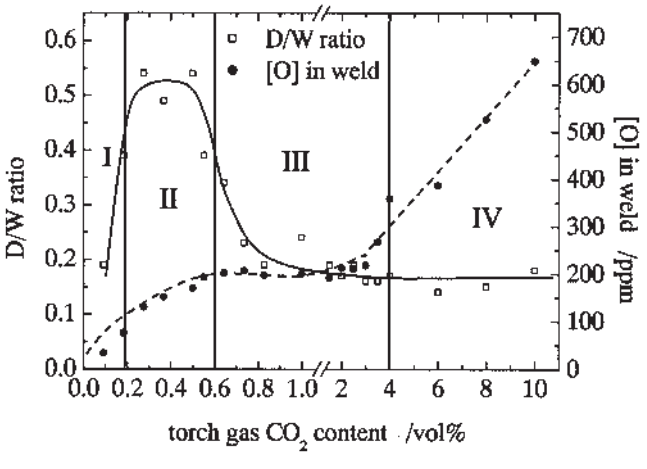


Fig. 3—Weld D/W ratio and oxygen content in weld *vs* torch gas $CO_2$ content.

that significantly influences the fluid flow in the liquid pool. Sahoo *et al*. studied the surface tension of binary metals and calculated the temperature coefficient of the surface tension for the Fe-O and Fe-S systems. They found that the temperature coefficient of the surface tension is always negative for a low oxygen content in iron (<20 ppm). On the other hand, for higher oxygen contents, it can change from a positive value at relatively low temperatures to a negative value at higher temperatures. Therefore, the Marangoni convection on the pool surface is complex, with a coexisting outward direction in the weld-pool center area and inward direction in the pool edge area when the oxygen in the iron is over 20 ppm. The critical temperature point on the weld-pool surface for an outward Marangoni convection change to an inward convection increases with the oxygen content, based on DebRoy and co-workers' results. The weld-pool peak temperature for SS304 stainless is from 2223 to 2673 K for a welding current from 50 to 200 A.[30] Based on these results, in the Fe-O system, the outward Marangoni convection in the pool center area may play the main role when the oxygen content is relatively low, whereas, when the oxygen content is higher, the inward convection outside of the pool center plays the main role on the pool surface. Generally, surface tension decreases with increasing temperature, $\partial\sigma/\partial T < 0$, for a pure metal and many alloys. Since there is a large temperature gradient existing on the welding-pool surface between the center under the torch and the edges of the weld pool, a large surface-tension gradient will be produced along the surface. In the weld pool for such materials, the surface tension is higher in the cooler part of the pool, at the edge, than in the pool center, under the arc, and, hence, the Marangoni convection flows from the pool center to the edge. The heat flux from the arc power in the pool center is easily transferred to the edge and the weld shape is relatively wide and shallow, as shown in Figure 4(a). When the surface-active elements, such as sulfur, oxygen, and selenium, exceed a certain value in stainless steel,[5,12] the temperature coefficient of the surface tension ($\partial\sigma/\partial T$) changes from a negative to a positive value, $\partial\sigma/\partial T > 0$, and the direction of the Marangoni convection on the weld pool changes,

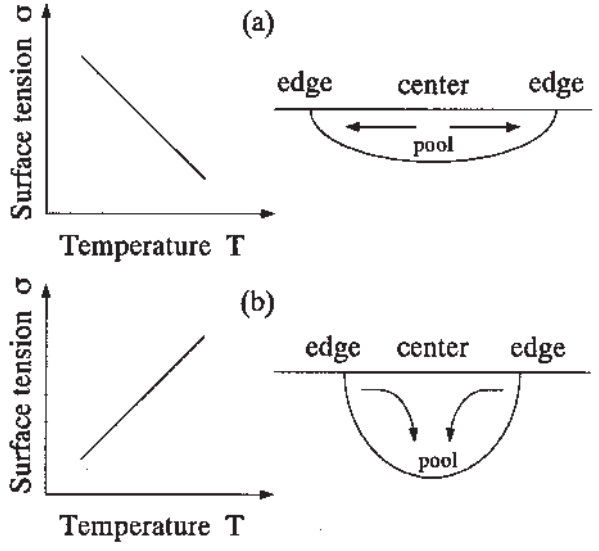


Fig. 4—Marangoni convection mode by surface tension gradient in welding pool: (*a*) $\partial\sigma/\partial T < 0$ and (*b*) $\partial\sigma/\partial T > 0$.

as illustrated in Figure 4(b). In this case, the heat flux easily transfers from the center to the bottom, and a relatively deep and narrow weld is made.

Oxygen from the decomposition of $CO_2$ provides a significant source of oxygen absorption for the molten weld metal in these experiments. The oxygen content in the weld pool increases with increasing $CO_2$ additions when the $CO_2$ content is below 0.6 vol pct and over 4.0 vol pct, as shown in areas I, II, and IV in Figure 3. Earlier research has shown that oxygen is an active element in pure iron and stainless steel in the range of 150 to 350 ppm[31] and 70 to 300 ppm.[25] In these ranges, the temperature coefficient of the surface tension of the welding pool is positive (inward convection in the weld pool), while outside of these ranges, the temperature coefficient of the surface tension becomes negative or nearly zero. When the oxygen content is over 80 ppm in the weld, the Marangoni convection mode is suddenly changed from outward to inward and the shallow-wide weld shape (low *D*/*W* ratio) changes to a narrow-deep weld shape (large *D*/*W* ratio), as shown in areas I and II in Figure 3. When the $CO_2$ content in the shielding gas is over 0.6 vol pct, the weld shape becomes wide and shallow again, as shown in areas III and IV in Figures 2 and 3. Furthermore, the oxygen content in the welding pool initially remains constant at 200 ppm, then continuously increases when the $CO_2$ content is over 4.0 vol pct.

### B. *Oxide Layer and Weld-Pool Motion*

In these experiments, carbon dioxide was mixed to the pure argon-based shielding gas. The addition of carbon dioxide to the argon shielding gas made the oxidation of the liquid weld-pool surface possible. Observations of the surface oxide layer were taken by laser microscopy. The group of pictures in Figure 5 shows the oxide layer on the weld surface. The

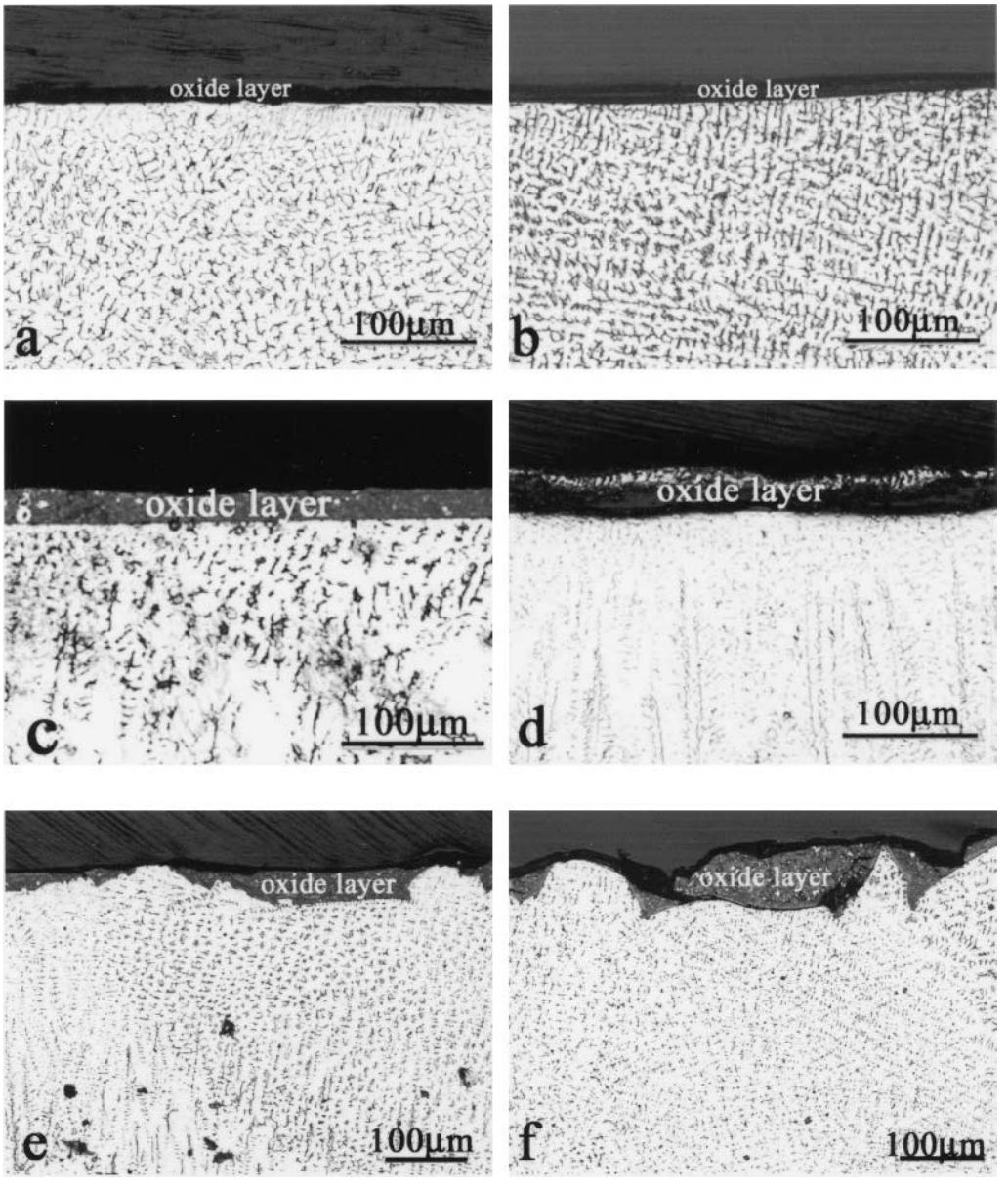


Fig. 5—Oxide layer on weld surface with different $CO_2$ contents in Ar shielding gas: (*a*) 0.092 vol pct, (*b*) 0.5 vol pct, (*c*) 0.736 vol pct, (*d*) 1.5 vol pct, (*e*) 6.0 vol pct, and (*f*) 8.0 vol pct.

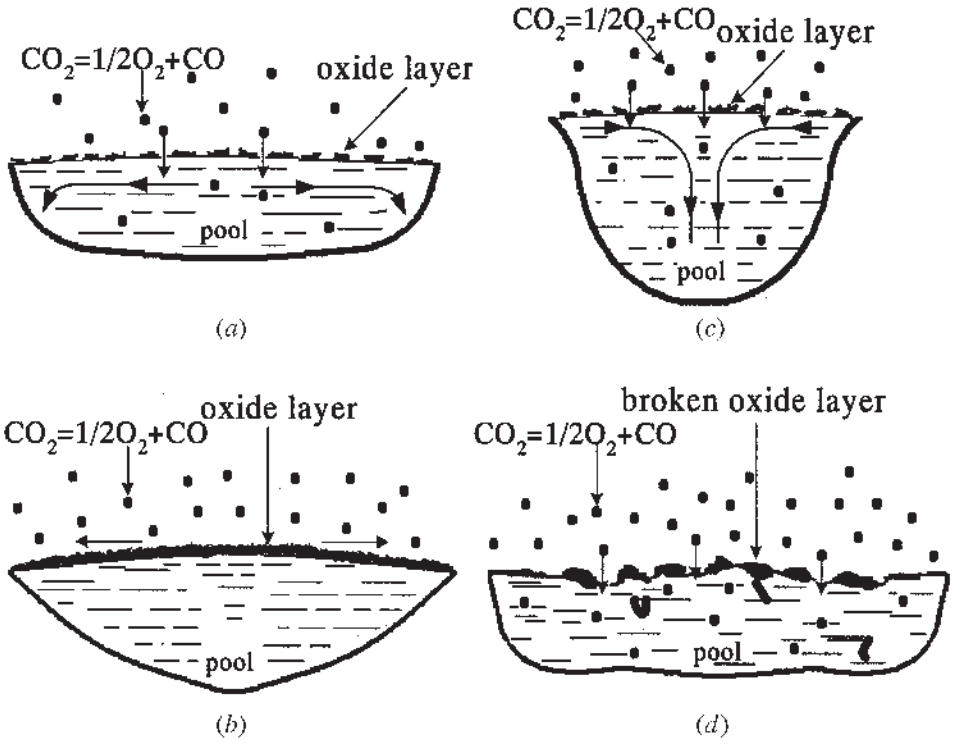


Fig. 6—Interaction mode between $CO_2$ oxide layer and weld pool: (*a*) and (*b*) quasi-free pool surface below 0.6 vol pct $CO_2$ additions, (*c*) restricted pool surface between 0.6 vol pct to 4.0 vol pct $CO_2$ additions, and (*d*) saw-toothed pool surface over 4.0 vol pct $CO_2$ additions.

oxide layer on the weld is thin at around 10 $\mu$m, as shown in Figures 5(a) and (b), when the $CO_2$ addition is lower than 0.6 vol pct. When the $CO_2$ addition is over 0.6 vol pct and below 4.0 vol pct, the oxide layer is suddenly increases to around 30 $\mu$m, as shown in Figures 5(c) and (d). Also, this heavy oxide layer prefers to locate in the periphery area of the bead surface. As the $CO_2$ addition reaches 4.0 vol pct, the weld-pool surface is uneven and becomes a saw-toothed surface under the torch. Furthermore, the oxide layer is broken, as shown in Figures 5(e) and (f).

In our experiments, as the $CO_2$ addition was between 0.6 vol pct (6000 ppm) and 4.0 vol pct, the oxygen in the weld pool is around 200 ppm, and the weld shape and weld *D*/*W* ratio changed from a spherical, deep cylindrical shape to a periphery shallow, concave-bottomed shape, as clearly shown in Figures 1 and 3 (areas II and III). In the pure inert-gas shielding GTA welding, the oxide slag is mainly from the floating of the inclusion in the weld pool, and the total amount of the slag is quite low. However, under the $CO_2$-Ar mixed shielding gas, the oxide layer on the weld surface can easily form on the liquid-pool surface by the carbon dioxide in the shielding gas, during the weld-pool solidification process, and even at higher temperatures after solidification.

One model to illustrate the effects of the oxide layers on the oxygen conveyance and weld-pool motion is proposed here and shown in Figure 6. A thin oxide layer around 10-$\mu$m thick formed on the welding-pool surface when the $CO_2$ addition was lower than 0.6 vol pct. This thin oxide layer can occur on the liquid-pool surface due to oxidation of $CO_2$ from the shielding gas. Since the welding-pool surface is not stationary and moves under the Marangoni convection force and the plasma shear force, the thin oxide layer is easily destroyed and exposes the liquid weld pool to the arc and shielding gas, as shown in Figures 6(a) and (b). In this case, the thin oxide layer will not inhibit the weld-pool motion severely, and the oxygen from the decomposition of $CO_2$ is possibly transferred and becomes dissolved in the welding pool. The welding-pool surface is in a quasi-free state. When the oxygen in the weld pool is over 80 ppm, the Marangoni convection of the liquid pool changes from outward to inward, and, hence, the wide shallow weld shape changes to a narrow deep shape, as shown in Figures 6(a) and (b). When the $CO_2$ addition is over 0.6 vol pct and below 4.0 vol pct, there is a heavy oxide layer covering the liquid-pool surface. This thick oxide layer is not easily destroyed by the pool motion and protects the liquid steel from direct contact with the shielding gas in the welding process, as shown in Figure 6(c). It becomes a barrier for oxygen conveyance to the weld pool. Therefore, the oxygen content does not increase when the $CO_2$ addition is over 0.6 vol pct, as shown in area III in Figure 3.

**Table III. Composition of the Heavy Oxide Layer on the Weld Surface (Atomic Percent)**

| Sample Weld Condition | O | Mn | Fe | Cr | Si | Al |
|---|---|---|---|---|---|---|
| With 0.74 vol pct $CO_2$-Ar shielding gas | 29.8 | 16.4 | 16.8 | 22.7 | 18.6 | 1.3 |
| | 31.1 | 12.9 | 9.0 | 25.0 | 21.0 | 1.1 |
| With 6.0 vol pct $CO_2$-Ar shielding gas | 33.3 | 11.1 | 10.0 | 23.5 | 21.1 | 1.0 |
| | 30.1 | 11.7 | 10.7 | 32.9 | 13.7 | 1.0 |

Table III shows the composition-analysis result by X-ray energy-dispersive spectroscopy of the heavy oxide layer formed on the weld-pool surface. Two samples were prepared and analyzed for each weld condition. The main elements in the oxide layer are oxygen, manganese, silicon,

chromium, iron, and a slight amount of aluminum. Ikemiya and co-workers[32] showed that the surface tensions of the molten single oxide at the melting points could be represented as a function of the electrostatic force ($F$) acting between a cation and oxygen. Oxides with strong cation-anion attractions (high $F$ value) easily form network formers. The temperature coefficient of the surface tension for molten oxides is related to their structures. Molten oxides with a network structure often change with the temperature and have a positive temperature coefficient of surface tension, such as $V_2O_5$, $SiO_2$, and $B_2O_3$. The electrostatic force of MnO, FeO, and $Cr_2O_3$ is low, so it is postulated that the temperature coefficient of surface tension of MnO, FeO, and $Cr_2O_3$ is negative. Calculation results by Boni and Derge[33] also showed that the temperature coefficients of the surface tension are negative for MnO and FeO and positive for $SiO_2$.

Since the heavy oxide layer on the welding-pool surface is manly composed of MnO, FeO, and $Cr_2O_3$ with a negative temperature coefficient of surface tension, it is assumed that the heavy oxide layer on the pool surface is assumed to have a negative temperature coefficient of surface tension. In the welding process, the center temperature under the torch is higher than that at the pool edges, so the liquid oxide layer will move in an outward direction, as shown in Figure 6(c). It may become a barrier for inward fluid flow of the weld pool beneath it. On the other hand, this continuous heavy oxide layer separated the liquid-pool surface from contacting with the gas, and the liquid-pool/gas interface does not exist. The liquid-pool/gas surface tension or Marangoni convection may no longer be the main factor any more in controlling the weld-pool flow. Therefore, the weld-pool shape changed to wide and shallow again, even when the oxygen content remained around 200 ppm.

It was found that when the $CO_2$ addition is greater than 4.0 vol pct, the arc was not stable and the electrode tip was partially melted during the welding process. The liquid-pool flow is controlled by the combination of the electromagnetic force, surface tension, impinging force of the arc plasma, and buoyancy. The unstable arc will make the fluid flow more complex, and the continuous heavy oxide was broken by the complex flow in the weld pool and formed an uneven pool surface like a saw-tooth, as shown in Figure 6(d). The broken oxide layer will expose the liquid-pool surface to the shielding gas, and the oxygen will transfer and continuously become a solute in the welding pool. Also, the complex flow possibly mixes the broken oxides in the weld pool. Therefore, the oxygen content in the weld pool increases again when the $CO_2$ addition is over 4.0 vol pct, as shown in area IV in Figure 3.

## IV. CONCLUSIONS

The addition of $CO_2$ gas to the argon base will significantly affect the weld-pool shape and penetration in the GTA welding of SUS304 steel. The weld shape changes from a shallow flat-bottomed shape, to a deep cylindrical shape, to a shallow concave-bottomed shape, and, finally, back to a shallow flat-bottomed shape when the $CO_2$ content in the weld pool is in the range of 0.092 to 10 vol pct. The weld $D/W$ ratio dramatically increases to 0.5 when the $CO_2$ addition is in the range of 0.2 to 0.6 vol pct. Higher or lower $CO_2$ additions will decrease the depth-to-width ratio to 0.2.

The weld-pool shape and penetration depend, to a large extent, on the liquid-pool convection mode. The Marangoni force is one of the main facts controlling the liquid-pool motion. Oxygen in the weld from the decomposition of carbon dioxide is an active element affecting the Marangoni convection mode. When the oxygen in the weld is over 80 ppm, the Marangoni convection is inward on the weld-pool surface. Lower than 80 ppm, it changes to an outward mode.

The oxide layer easily forms on the pool surface under the $CO_2$-Ar mixed-gas shielding. The thick oxide layer protects the liquid pool from being exposed to the shielding gas and becomes a barrier for the oxygen conveyance to the welding pool. Also, the heavy oxide layer separates the liquid pool from contacting with the gas, and the liquid-pool/gas surface tension or Marangoni convection may no longer be the main factor controlling the liquid-pool convection.

## ACKNOWLEDGMENTS

This work is the result of "Development of Highly Efficient and Reliable Welding Technology," which is supported by the New Energy and Industrial Technology Development Organization (NEDO, 01MB7) through the Japan Space Utilization Promotion Center (JSUP) in the program of Ministry of Economy, Trade and Industry (METI), ISIJ research promotion grant, Japan Steel Engineering grant (JFE), and the 21st Century Center of Excellence (COE) Program.

## REFERENCES

1. H.C. Lugwig: *Welding J.,* 1957, vol. 36, pp. 335s-341s.
2. B.E. Paton: *Avtom. Svarka*., 1974, No. 6, pp. 1-4.
3. W.S. Bennett and G.S. Mills: *Welding J*., 1974, vol. 53, pp. 548s-553s.
4. W.F. Savage, E.F. Nippes, and G.M. Goodwin: *Welding J*., 1977, vol. 56, pp. 126s-132s.
5. C.R. Heiple and J.R. Roper: *Welding J*., 1981, vol. 60, pp. 143s-145s.
6. Y. Takeuchi, R. Takagi, and T. Shinoda: *Welding J*., 1992, vol. 71, pp. 283s-289s.
7. M. Tanaka, T. Shimizu, H. Terasaki, M. Ushio, F. Koshi-ishi, and C.L. Yang: *Sci. Technol. Welding Joining*, 2000, vol. 5, pp. 397-402.
8. P.J. Modenesi, E.R. Apolinario, and I.M. Pereira: *J. Mater. Proc. Technol*., 2000, vol. 99, pp. 260-65.
9. M. Kuo, Z. Sun, and D. Pan: *Sci. Technol. Welding Joining*, 2001, vol. 6, pp. 17-22.
10 D. Fan, R. Zhang, Y. Gu, and M. Ushio: *Trans. JWRI*, 2001, vol. 30, pp. 35-40.
11. D.S. Howse and W. Lucas: *Sci. Technol. Welding Joining*, 2000, vol. 5, pp. 189-93.
12. C.R. Heiple and J.R. Roper: *Welding J*., 1982, vol. 61, pp. 97s-102s.
13. P.C.J. Anderson and R. Wiktorowicz: *Welding Met. Fabr*., 1996, vol. 64, pp. 108-09.
14. W. Lucas and D. Howse: *Welding Met. Fabr*., 1996, vol. 64, pp. 11-17.
15. D.D. Schwemmer, D.L. Olson, and D.L. Williamson: *Welding J*., 1979, vol. 58, pp. 153s-160s.
16. F. Liu, S. Lin, C. Yang, and L. Wu: *Trans. China Welding Inst*., 2002, vol. 23, pp. 1-4.
17. T. Paskell, C. Lundin, and H. Castner: *Welding J*., 1997, vol. 76, pp. 57-62.
18. F. Liu, S. Lin, C. Yang, and L. Wu: *Trans. China Welding Inst*., 2002, vol. 23, pp. 5-8.
19. Y. Wang and H.L. Tsai: *Metall. Mater. Trans. B*, 2001, vol. 32B, pp. 501-15.
20. S.P. Lu, H. Fujii, H. Sugiyama, M. Tanaka, and K. Nogi: *Trans. JWRI*, 2003, vol. 32, pp. 79-82.
21. B.N. Bad'yanov: *Avtom. Svarka*., 1975, No. 1, p. 75.
22. C.R. Heiple and P. Burgardt: *Welding J*., 1985, vol. 64, pp. 159s-162s.
23. S.P. Lu, H. Fujii, H. Sugiyama, M. Tanaka, and K. Nogi: *Iron Steel Inst. Jpn. Int*., 2003, vol. 43, pp. 1590-95.
24. S.M. Gurevich and V.N. Zamkov: *Avtom. Syarka*., 1966, vol. 12, pp. 13-16.

25. S.P. Lu, H. Fujii, H. Sugiyama, M. Tanaka, and K. Nogi: *Mater. Trans*., 2002, vol. 43, pp. 2926-31.
26. S.P. Lu, H. Fujii, H. Sugiyama, and K. Nogi: *Metall. Mater. Trans. A*, 2003, vol. 34A, pp. 1901-07.
27. K.C. Mills, B.J. Keene, R.F. Brooks, and A. Shirali: *Phil. Trans. R. Soc. London*, 1988, vol. 356A, pp. 911-25.
28. P. Sahoo, T. DebRoy, and M.J. McNallan: *Metall. Trans. B*, 1988, vol. 19B, pp. 483-91.
29. K. Ishizaki, N. Araki, and H. Murai: *J. Jpn. Welding Soc*., 1965, vol. 34, pp. 146-53.
30. H.G. Kraus: *Welding J*., 1989, vol. 68, pp. 269s-79s.
31. H. Taimatsu, K. Nogi, and K. Ogino: *J. High. Temp. Soc*., 1992, vol. 18, pp. 14-19.
32. N. Ikemiya, J. Umemoto, S. Hara, and K. Ogino: *Iron Steel Inst. Jpn. Int*., 1993, vol. 33, pp. 156-65.
33. R.E. Boni and G. Derge: *J. Met*., 1956, vol. 8, pp. 53-59.